arXiv:2107.12100v1 [cs.SI] 26 Jul 2021

Predicting Influential Higher-Order Patterns in Temporal Network Data

Christoph Gote[1,4]   **Vincenzo Perri**[2,5]   **Ingo Scholtes**[2,3]

[1]*Chair of Systems Design, ETH Zurich, Zurich, Switzerland*
[2]*Data Analytics Group, University of Zurich, Zurich, Switzerland*
[3]*Chair of Data Analytics, Univerity of Wuppertal, Wuppertal, Germany*

[4]*cgote@ethz.ch*
[5]*perri@ifi.uzh.ch*

Abstract

Networks are frequently used to model complex systems comprised of interacting elements. While links capture the topology of *direct* interactions, the true complexity of many systems originates from higher-order patterns in paths by which nodes can *indirectly* influence each other. Path data, representing ordered sequences of consecutive direct interactions, can be used to model these patterns. However, to avoid overfitting, such models should only consider those higher-order patterns for which the data provide sufficient statistical evidence. On the other hand, we hypothesise that network models, which capture only direct interactions, underfit higher-order patterns present in data. Consequently, both approaches are likely to misidentify influential nodes in complex networks. We contribute to this issue by proposing eight centrality measures based on MOGen, a multi-order generative model that accounts for all paths up to a maximum distance but disregards paths at higher distances. We compare MOGen-based centralities to equivalent measures for network models and path data in a prediction experiment where we aim to identify influential nodes in out-of-sample data. Our results show strong evidence supporting our hypothesis. MOGen consistently outperforms both the network model and path-based prediction. We further show that the performance difference between MOGen and the path-based approach disappears if we have sufficient observations, confirming that the error is due to overfitting.

Keywords: Higher-Order Networks, Path Analysis, Centrality Measures

---

Both corresponding authors contributed equally to this paper.

1   Introduction

Network models have become an important foundation for the analysis of complex systems across various disciplines, including physics, computer science, biology, economics, and the social sciences [31]. To this end, we commonly utilise graphical models of complex systems that consist of many interacting elements, where the *nodes* or *vertices* of the graph represent the elements, and *links* or *edges* of the graph represent dyadic interactions between those elements. A significant contribution of this perspective on complex systems is that it provides a unified mathematical language to study how the topology of the interactions between individual elements influences the macroscopic structure of a system or the evolution of dynamical processes [4].

In a network, links capture the *direct* influence between adjacent nodes. However, for most networked systems with sparse interaction topologies, the true complexity originates from higher-order patterns capturing *indirect* influence mediated via *paths*, i.e., via sequences of incident links traversed by dynamical processes. The general importance of paths for analysing complex systems is expressed in many standard techniques in social network analysis and graph theory. Examples include measures for the importance of nodes based on shortest paths [3, 10], methods for the detection of community structures that are based on paths generated by random walkers [23], but also algebraic and spectral methods that are based on powers of adjacency matrices or the eigenvalues of graph Laplacians [7], which can be thought as implicitly expanding links into paths.

Standard network methods typically analyse systems based on paths that are generated by some model or algorithm operating on the network topology, e.g., shortest paths calculated by an algorithm, random paths generated by a stochastic model, or all paths transitively expanded based on the network topology. The choice of a suitable model or process generating those paths is a crucial step in network analysis, e.g., for the assessment of node importance [5]. On the other hand, rather than using paths generated by models, we often have access to time-series data that captures real paths in networked systems. Examples include human behavioural data such as time-stamped social interactions, clickstreams on websites, or travel itineraries in transportation networks.

Recent works have shown that, for many complex systems, the patterns in time series data capturing such paths cannot be explained by the network topology alone. They instead contain higher-order patterns that influence the causal topology of a system, i.e., who can indirectly influence whom over time. To capture these patterns, higher-order generalisations of network models have been proposed [2, 14, 33]. While the specific assumptions about the type of higher-order structures included in those models differ, they have in common that they generalise network models towards representations that go beyond pairwise, dyadic interactions. Recent works in this area have used higher-order models for non-Markovian patterns in paths on networks to study random walks and diffusion processes [15,

24, 29], detect communities and assess node centralities [8, 21, 24, 28, 36], analyse memory effects in clinical time series data [13, 18, 20], generate node embeddings and network visualisations based on temporal network data [22, 25, 32], detect anomalies in time series data on networks [16, 26], or assess the controllability of complex systems [37]. Moreover, recent works have shown the benefit of *multi-order models* that combine multiple higher-order models, e.g., for the generalisation of PageRank to time series data [27] or the prediction of paths [12].

Extending this view, in this work, we propose eight centrality measures to identify influential nodes and node sequences based on a multi-order generative model trained on path data. We argue that for this purpose, it is essential to account for the fact that paths are ordered finite-length sequences with a specific start and end node. We show that paths generated based on standard network models underfit the patterns in data on real observed paths. In contrast, a direct calculation of centrality measures based on those paths leads to overfitting expressed in the misidentification of influential nodes or node sequences. We instead compute centralities based on MOGen, a multi-order generative model of paths capable of learning only those patterns for which a set of path data contains sufficient statistical evidence [12].

The contributions of our work are as follows:

- We consider eight centrality measures for nodes in complex networks and generalise them to a multi-order generative model for paths in complex networks. Those measures can be considered proxies for the influence of specific node sequences on dynamical processes like, e.g., epidemic spreading and information propagation.

- We show that the direct use of observed paths to calculate those centralities yields better predictions of influential nodes in time series data than a simpler network-based model if there is sufficient training data. At the same time, this approach introduces a substantial generalisation error for small data sets. This motivates the need for a modelling approach that balances between under- and overfitting.

- We develop a prediction technique based on a probabilistic graphical model that integrates Markov chain models of multiple higher orders. Unlike previous works that used multi-order models to model paths in networks, our framework explicitly models the start and end nodes of paths. We show that this explicit modelling of start/end probabilities is crucial to predict influential node sequences.

- Using five empirical data sets on variable-length paths in human clickstreams on the Web, passenger trajectories in transportation systems, and interaction sequences in time-stamped contact networks, we show that our approach provides superior prediction performance.

2   Methods

In the following, we introduce our approach to predict influential nodes and higher-order patterns based on MOGen, a multi-order generative model for path data [12]. To this end, we first introduce and contrast network and path data and discuss the different types of patterns they can capture. Based on this, we then motivate the need for a multi-order model such as MOGen that captures the start- and endpoints of paths and patterns in the order in which nodes are traversed in networked systems. After providing an overview of the MOGen model, we apply Markov chain theory to derive the Fundamental matrix of the MOGen model. Based on this Fundamental matrix, we finally introduce eight centrality measures capturing different notions of influence. We discuss how all centrality measures can be computed based on a MOGen model. In addition, we also provide methods to compute them based on a network representation and path data, as we are using those in our comparison in Section 4. For all measures, we explain how we can project centralities computed for higher-order nodes—i.e., node sequences—back to first-order nodes, i.e., nodes in the original network.

2.1   Paths on Network Topologies

We mathematically define a *network* as tuple $G = (V, E)$, where V is a set of nodes and E is a set of edges. In the example of a public transport system, the individual stations are the nodes, and a link exists between two nodes if there is a direct connection between the two stations. Users of the system move from start to destinations following *paths* that are restricted by the network topology. A *path* is defined as an ordered sequence $s = v_1 \rightarrow v_2 \rightarrow \cdots \rightarrow v_{l_s}$ of nodes $v_i \in V$, where l_s is the length of the path. Importantly, different from other definitions of paths in graph theory, we assume that the same node can appear more than once in that sequence. We refer to a set of paths constrained by the same network topology as path data set P.

While empirical paths can come from various sources, we can differentiate between two main types: (i) data directly recorded in the form of paths; (ii) paths extracted from data on temporal interactions, i.e., a temporal network. Examples for the first case include clickstreams of users on the Web or data capturing passenger itineraries from public transportation systems. The primary example of temporal data are records on human interactions, which are a common source for studying knowledge transfer or disease transmission.

A *temporal network* is a tuple $G^{(t)} = (V, E^{(t)})$, where V is a set of vertices and $E^{(t)}$ is a set of edges with a time stamp $E^{(t)} \subseteq V \times V \times \mathbb{N}$. We can extract paths from a temporal network by setting two conditions. First, for two time edges $e_i = (v_1, v_2; t_1)$ and $e_j = (v_2, v_3; t_2)$ to be considered consecutive in a path—i.e., $s = \cdots \rightarrow v_1 \rightarrow v_2 \rightarrow v_3 \rightarrow \cdots$—they have to respect the arrow of time, i.e., $t_1 < t_2$. Second, consecutive

interactions belong to the same path only if they occur within a time window δ, i.e., $t_2 - t_1 \leq \delta$. Using these conditions, we can derive a set of paths P from any temporal network.

Besides obtaining paths from empirical observations, we can also *generate* paths based on a network topology. A convenient way to generate paths is to simulate finite length random walks on the network. A walk starts at node $v_1 \in V$ and continues through a sequence of nodes v_i, $i \geq 2$, fulfilling the condition that all successive nodes can be reached from their predecessors through a single link, i.e., $e = (v_i, v_{i+1}) \in E$. A path ends either after a certain length $l_p \geq 1$ is reached or if no further transitions are possible as no links from v_i exist.

Empirical paths are important because their properties can differ significantly from those of paths obtained based on random walk models. These differences originate from two assumptions we need to make when generating paths with walks. First, we have to make assumptions on the start- and endpoints of paths and the path lengths, as the network topology does not include any information on these properties. Second, by randomly following links on the network topology, we commonly assume that nodes are traversed in a memoryless fashion. In other words, we assume that the next node visited on a path is only conditional on the current node, i.e., paths are Markovian.

Going back to our example of the transportation system, we can easily see that generating paths from the topology oversimplifies the system's dynamics. While it is not apparent from the network topology, *empirical* paths are more likely to start and end in some nodes (i.e., stations) than others. In addition, when travelling from destination to target, users are more likely to move away from nodes they have already visited, as they are moving away from a source node to reach a target node.

In summary, the network topology constrains the paths that are possible in real-world systems, such as transport or communication systems. However, empirical path data contain additional information on the start and endpoints of paths and the sequences in which nodes are traversed that the network topology does not capture.

2.2   Modelling Higher-Order Patterns in Path Data

In the previous section, we showed that empirical paths capture information not contained in the network topology. Based on our arguments, one might assume that paths are always better to capture the dynamics on a networked system compared to the topology alone. However, the validity of this argument strongly depends on the number of paths that we have observed.

Let us consider the simple toy example shown in Figure 1. As we can infer from the colour coded paths, a path in D will always continue to E if it started in A. In contrast, if the path started in B, it will continue to F. But does this mean that paths from A to F do not exist, despite being possible according to the underlying network topology? To address this question, we need to consider how
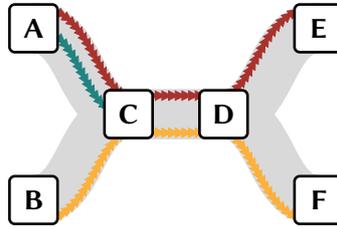
Figure 1: Exemplary set of paths on a network topology. We observe three colour coded paths from *A* to *B* (■), from *A* to *E* (■), and from *B* to *F* (■). The underlying network topology is shown in grey (■)

often we observed the paths from *A* to *E* and *B* to *F*. If, e.g., we observed both paths only once each, we would have little evidence suggesting that a path from *A* to *F* would not be possible. Hence, in this case, using the observed paths as indicators for all possible paths would overfit the data, and a network model would be more appropriate. In contrast, observing both paths many times without ever observing paths from *A* to *F* would indicate that paths from *A* to *F* do not exist or are at least significantly less likely than the observed paths. In this case, a network model would underfit the data by not adequately accounting for the patterns present in the empirical path data.

These examples underline that to capture the influence of nodes in real-world networked systems, neither a network model nor a limited set of observed paths is sufficient. Instead, we require a model that can both represent the non-Markovian patterns in the path data, and allow transitions that are consistent with the network topology and cannot be ruled out because path data have not provided enough evidence.

The modelling of non-Markovian sequences on networks has been addressed by the higher-order network community. Treating the transitions on a network as transitions between the states of a Markov chain, higher-order models are naturally equipped to address non-Markovianity using the methods developed for higher-order Markov chains. In these models, the influence of previous transitions on a coming one is modelled by grouping together sequences of nodes in so-called *higher-order nodes*. In a network of order k, also referred to as k-th order network, a path of length l is not a sequence of $l-1$ transitions between nodes. Instead, it is turned into a sequence of $l-k+1$ transitions between k-th order nodes, where each k-th order node represents an ordered sequence of k traversed nodes or $k-1$ traversed links. For instance, in a third order network, the paths $A \rightarrow C \rightarrow D \rightarrow E$ and $B \rightarrow C \rightarrow D \rightarrow F$ from the example in Figure 1 become

$$(A, C, D) \rightarrow (C, D, E),$$
$$(B, C, D) \rightarrow (C, D, F),$$

constrained by a third-order network topology with nodes (A, C, D), (C, D, E), (B, C, D), (C, D, F) and transition probabilities

$$p\{(A, C, D) \rightarrow (C, D, E)\} = 1,$$
$$p\{(B, C, D) \rightarrow (C, D, F)\} = 1,$$
$$p\{(A, C, D) \rightarrow (C, D, F)\} = 0,$$
$$p\{(B, C, D) \rightarrow (C, D, E)\} = 0.$$

2.3 MOGen

Different from the non-Markovianity, the modelling of start- and endpoints of paths has received little attention. However, recently the authors of [12] developed MOGen, a multi-order generative model of paths combining the information from multiple higher-order models while simultaneously explicitly considering the start- and endpoints of paths. The maximum length of the higher-order patterns considered by MOGen is defined by the maximum order K, the only parameter of the model. A MOGen model with $K = 3$ for the training data in our example is shown in Figure 2.

Modelling both the start and end probabilities of paths and higher-order patterns, MOGen provides a comprehensive representation of the patterns in path data. When learning a MOGen model from a set of path data P, we use a special *initial state* ✷, with transitions ✷ $\rightarrow v$ to first-order nodes $v \in V$ that represent the start of a path in node v. From here, we model transitions to subsequent higher-order nodes up to the maximum-order K of the multi-order model. For all orders $1 \leq k \leq K$, we further add transitions from k-th order nodes $(v_1, \dots, v_k) \rightarrow$ ✚ to a special *terminal state* ✚, which captures the termination of a path. With this extension, a path $v_1 \rightarrow v_2 \rightarrow \cdots \rightarrow v_l$ corresponds to $l + 2$ transitions in a *multi-order network* with maximum order K, which gives rise to the following sequence of l higher-order nodes:

$$\text{✷} \rightarrow v_1 \rightarrow (v_1, v_2) \rightarrow (v_1, v_2, v_3) \rightarrow \cdots \rightarrow (v_{l-K+1}, \dots, v_l) \rightarrow \text{✚}. \tag{1}$$
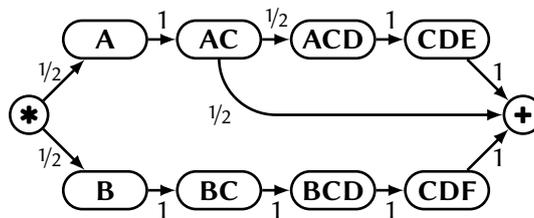

Figure 2: MOGen model with $K = 2$ for the exemplary set of paths shown in Figure 1.

$$
\mathbf{A}^{(K)} =
\begin{array}{c}
\quad\ \ V^1 \quad V^2 \quad \cdots \quad V^K \quad\ + \\
\begin{array}{c}
\ast \\
V^1 \\
\vdots \\
V^{K-1} \\
V^K
\end{array}
\left(
\begin{array}{ccccc}
\mathbf{A}_{0,1} & & 0 & & 0 \\
& \mathbf{A}_{1,2} & & & \\
& & \vdots & 0 & \mathbf{A}_+ \\
& & & \mathbf{A}_{K-1,K} & \\
& 0 & & \mathbf{A}_{K,K} & \\
\end{array}
\right)
\end{array}
$$

Figure 3: Multi-order adjacency matrix of MOGen with maximum-order K.

Both the network model and the complete set of paths can be represented as special cases of MOGen. A first-order MOGen model ($K = 1$) without the initial and terminal nodes ✱ and ✚ corresponds to the network representation of the paths. A MOGen model for which the maximum order is equal to the maximum path length observed in P is a lossless representation of the set of paths. When there is sufficient evidence for specific higher-order patterns but not for others, MOGen models with maximum orders lower than the maximum path length can be used to restrict some transitions while simultaneously allowing for other transitions not observed in the training data. MOGen facilitates the search for the *optimal* order K by deriving a set of multi-order models $M^{(k)}$, $k \in \mathrm{N}^+$ and selecting the model among this set using AIC-based model selection.

Thus, MOGen allows us to find a balance between the network model—allowing all observed transitions in any order—and the observed set of paths—only allowing for transitions in the order in which they were observed. Coming back to the example shown in Figure 1 a MOGen model with $K = 2$ would capture that paths can end in C when originating in A but not when originating in B. However, it would allow for the existence of paths from A to F.

In Section 4, we will test MOGen's capability to capture the non-Markovian patterns present in real-world networked systems. To this end, we will learn MOGen models with different maximum orders based on a set of training paths. We will then use the models to predict influential nodes and higher-order patterns and validate the predictions in out-of-sample test data. We will contrast the results of MOGen with predictions based on a network model and the complete training paths.

To allow this comparison, we now introduce a set of eight centrality measures and discuss how we can compute them for the MOGen model, a network model, and based on a set of paths.

Figure 4: Split of $\mathbf{T}^{(K)}$ into transient part $\mathbf{Q}$ and absorbing part $\mathbf{R}$. $\mathbf{S}$ represents the starting distribution of paths.

MOGen: Fundamental matrix. A MOGen model is fully described by a multi-order adjacency matrix $\mathbf{A}^{(k)}$ shown in Figure 3. Row-normalisation of $\mathbf{A}^{(K)}$ yields the multi-order transition matrix $\mathbf{T}^{(K)}$ capturing the probability of a transition between two higher-order nodes. As shown in Equation (1), MOGen represents the start and end of a path through the special states ✱ and ✚. This allows us to interpret the multi-order transition matrix $\mathbf{T}^{(K)}$ of MOGen as an absorbing Markov chain where the states $(v_1, \dots, v_{n-1}, v_n)$ represent a path in node v_n having previously traversed nodes $v_1, \dots, v_{n-1}$. Using this interpretation as a Markov chain allows us to split $\mathbf{T}^{(K)}$ into a transient part $\mathbf{Q}$ representing the transitions to different nodes on the paths and an absorbing part $\mathbf{R}$ describing the transitions to the end state ✚. We can further extract the starting distribution $\mathbf{S}$. All properties are represented in Figure 4.

This representation further allows us to compute the Fundamental matrix $\mathbf{F}$ of the corresponding Markov chain.

$$\mathbf{F} = \left(\mathbf{I}^{(n \times n)} - \mathbf{Q}\right)^{-1} \tag{2}$$

Here, $\mathbf{I}^{(n \times n)}$ is the $n \times n$ identity matrix, where n is the number of nodes in the multi-order model without counting the special states ✱ and ✚. Entries (i, j) of this Fundamental matrix F represent the expected number of times a path in node i will visit node j before ending. The Fundamental matrix F is essential as it allows us to compute path centrality measures for the MOGen model analytically.

2.4 Centrality measures

We now introduce eight MOGen-based centrality measures that we use in our comparison. For all MOGen-based centrality measures, we also introduce the corresponding measures for the network and a set of paths.

2.4.1 Visitation Probability

Often, we are interested in the frequency with which nodes in a system are visited. In transportation systems, this information allows us to estimate capacity requirements for airports or stations, whereas, for clickstream data, it gives us information about the importance of an individual website.

Mathematically, the visitation probability π_v of a node v is given by the probability of randomly picking exactly this node from any path p in the path data set P. This metric is proportional to the number of times a node was observed in any path, and it can be computed on a set of paths by simply counting and normalising the occurrences of a node.

$$\pi_v^{(P)} = \frac{\sum_{p \in S} \sum_{w \in p} \delta(w, v)}{\sum_{p \in S} |p|}, \qquad \delta(w, v) = \begin{cases} 1 & w = v \\ 0 & w \neq v \end{cases} \tag{3}$$

Here, $|p|$ is the number of nodes in a path p.

Analogously, for MOGen the visitation probability can be computed as the normalised column sums of the adjacency matrix $\mathbf{A}$.

$$\pi_v^{(M)} = \left(\frac{\mathbf{1}^{(1 \times n)} \times \mathbf{A}}{\mathbf{1}^{(1 \times n)} \times \mathbf{A} \times \mathbf{1}^{(n \times 1)}} \right)_v \tag{4}$$

Here, $\mathbf{1}^{(a \times b)}$ represents a matrix of ones of size a times b and n the number of higher-order nodes in $\mathbf{A}$. Equation (4) allows us to compute the visitation probability of all higher-order nodes or node sequences up to length K in the system. The visitation probability of a first-order node v can be obtained as the sum of all corresponding higher-order nodes, where all higher-order nodes ending in v correspond to v.

For networks, PageRank [19] is commonly used to compute the importance of a node in terms of visitation probability. PageRank returns the stationary state of a random walk on the network topology uniformly following links with probability d and *teleporting* to random nodes, without the requirement to follow an existing link, with probability $1 - d$ or if the current node has an out-degree of zero. This assumption is similar to paths ending and starting for both the path and MOGen models. We use $d = 0.85$ as commonly assumed in literature [19]. The resulting stationary distribution represents the visitation probability of all nodes, given the assumptions made for the random walk process.

PageRank can be computed as

$$\pi_v^{(N)} = \frac{1 - d}{|V|} + d \sum_{w \in V} \frac{\pi_w^{(N)}}{d_o(w)}, \tag{5}$$

where $d_o(w)$ is the out-degree of node w. We solve Equation (5) by applying the power method [1] to iteratively compute the PageRank of all nodes.

2.4.2 Betweenness Centrality

Betweenness centrality considers nodes as highly important if they frequently occur on paths connecting pairs of other nodes. In a network, the betweenness centrality of a node v is given by the ratio of shortest paths $\sigma_{st}(v)$ from s to t through v to all shortest paths from s to t σ_{st} for all pairs of nodes s and t:

$$b_v^{(N)} = \sum \frac{\sigma_{st}(v)}{\sigma_{st}}. \tag{6}$$

Standard betweenness centrality calculated in a network model relies on the assumption that only shortest paths are used to connect two nodes. Using actual path data, we can drop this assumption and consider paths that are actually used. Therefore, we can obtain the betweenness of a node in a given set of paths P by simply counting how many times a node appears between the first and last node of all paths.

For MOGen, we can utilise the properties of the Fundamental matrix F. Entries (v, w) of F represent the number of times we expect to observe a node w on a path continuing from v before the path ends. Hence, by multiplying F with the starting distribution S, we obtain a vector containing the expected number of visits to a node on any path. To match the notions of betweenness for networks and paths, we subtract the start and end probabilities of all nodes yielding

$$b_v^{(M)} = (\mathbf{S} \times \mathbf{F})_v - s_v - e_v^{(M)} \tag{7}$$

Similar to the visitation probability, nodes for MOGen are higher-order nodes. The betweenness centrality of a first-order node can be obtained as the sum of the corresponding higher-order nodes.

2.4.3 Closeness Centrality (Harmonic)

When considering the closeness centrality of a node v, we aim to capture how easily node v can be reached by other nodes in the network. For networks, we are therefore interested in a function of the distance of all nodes to the target node v. The distance matrix $\mathbf{D}$ capturing the shortest distances between all pairs of nodes can be obtained, e.g., by taking powers of the binary adjacency matrix of the network where the entries at the power l represent the existence of at least one path of length l between two nodes. This computation can be significantly sped up by using graph search algorithms such as the Floyd-Warshall algorithm [9] used in our implementation. As our networks are based on path data,

the resulting network topologies are directed and not necessarily connected. We, therefore, adopt the definition of closeness centrality for unconnected graphs, also referred to as harmonic centrality [17]. This allows us to compute the closeness centrality of a node v as

$$c_v^{(M)} = \sum_{d \in \mathbf{D}_v} \frac{1}{d}, \tag{8}$$

where $\mathbf{D}_v$ is the v-th row of $\mathbf{D}$.

As MOGen models contain different higher-order nodes, $\mathbf{D}$ captures the distances between higher-order nodes based on the multi-order network topology considering correlations up to length K. While we aim to maintain the network constraints set by the multi-order topology, we are interested in computing the closeness centralities for first-order nodes. We can achieve this by projecting the distance matrix to its first-order form, containing the distances between any pair of first-order nodes but constrained by the multi-order topology. For example, for the distances $d\{(A, B), (C, A)\} = 3$ and $d\{(B, B), (C, A)\} = 2$, the distance between the first-order nodes B and A is 2. Hence, while for the network, the distances are computed based on the shortest path assumption, multi-order models with increasing maximum order K allow us to capture the tendency of actual paths to deviate from this shortest path. Based on the resulting distance matrix $\mathbf{D}$, closeness centrality can be computed following Equation (8).

Finally, for paths, the distance between two nodes v and w can be obtained from the length of the shortest sub-path starting in v and ending in w among all given paths. Again, the closeness centrality is then computed using Equation (8). Therefore, while for all representations, we compute the closeness centrality of a node using the same formula, the differences in the results originate from the constraints in the topologies considered when obtaining the distance matrix $\mathbf{D}$.

2.4.4   Reach Centrality

While the closeness centrality captures the distance of a node to all other nodes, the reach centrality addresses the question of how many nodes can be reached up to a given distance d_{max}. For all three representations the distance matrix $\mathbf{D}$ is computed analogously to the closeness centrality. Then, the reach centrality of a node v is computed as

$$r_v = \sum (\mathbf{D} \le d_{max})_v. \tag{9}$$

For all analyses performed in this work, we consider all possible distances at which nodes can be reached, i.e., $\lim_{d_{max} \to \infty} r_v$. Similar to the closeness centrality, the different levels of higher-order con-

straints considered in the computation of the distance matrices D yield different values for the reach centralities for MOGen models with different K.

2.4.5 Path End Probability

The path end probability e_v of a node v describes the probability of a path to end in node v. For paths, $e_v^{(E)}$ is computed correspondingly by counting the fraction of paths ending in node v. For MOGen, all paths end with the state ✚. Therefore, $e_v^{(M)}$ is obtained from the transition probabilities to ✚ of a single path starting in ✱. This last transition can—and is likely to—be made from a higher-order node. We can obtain the end probability for a first-order node by summing the end probabilities of all corresponding higher-order nodes. Similar to the path start probability, e_v cannot be computed for first-order network models.

2.4.6 Path Continuation Probability

When following the transitions on a path, at each point, the path can either continue or end. With the path continuation probability f_v, we capture the likelihood of the path to continue from node v. Similarly to the path start and end probabilities, we obtain the path continuation probability from a set of paths P by counting the fraction of times v does not appear as the last node on a path compared to all occurrences of v.

For MOGen, the path continuation probability is given directly by summing the probabilities of all transitions in the row of $T^{(K)}$ corresponding to node v leading to the terminal state ✚. As for other measures, for MOGen, the continuation probabilities are computed for higher-order nodes. We can obtain continuation probabilities for a first-order node v as the weighted average of the continuation probabilities of the corresponding higher-order nodes, where weights are assigned based on the relative visitation probabilities of the higher-order nodes computed according to Equation (4) As path information is required, no comparable measure exists for networks.

2.4.7 Path Closeness

Earlier, when considering the closeness of a node v, we discussed that we want to capture how easily a node v can be reached by other nodes in the network. We did this by looking at a function of the distances of all nodes to node v. Taking a path perspective, we can also argue that v is close to other nodes if it is often reached by paths going through other nodes before the path ends. This is what we aim to capture with the notion of path closeness. For a set of paths, this requires us to obtain a normalised count of how often a node appears on a path, excluding the first node. For MOGen, however, we can utilise the Fundamental matrix F introduced in Section 4. Entries (v, w) of this matrix represent the

expected number of times a node w will be visited on a path currently in v before the path ends. Using this property, we can compute the path closeness of a node v as the weighted column sum of F, where the weights represent the visitation probabilities of all nodes.

$$\gamma_v^{(M)} = \left(\mathbf{F}^\top\right)_v \times \pi^{(M)} \tag{10}$$

The path closeness for first-order nodes is obtained as the sum of the path closeness of all corresponding higher-order nodes. Path closeness cannot be computed for networks as the information of endpoints is not available there.

2.4.8 Path Reach

Finally, we consider path reach. Similar to the standard reach centrality, we aim to address how many nodes can be reached from a node v, but from the perspective of path data. With path reach, we capture how many more transitions we expect to observe on a path currently in node v before it ends. To compute path reach for a set of paths P, we count the average number of nodes on all paths before the path ends for all nodes, in a procedure very similar to the one used to compute path closeness. For MOGen, we can again use the properties of the Fundamental matrix F and obtain the expected number as the row sum

$$\rho_v^{(M)} = \sum \mathbf{F}_v - 1 \tag{11}$$

We subtract 1 to discount for the occurrence of node v at the start of the remaining path. Analogous to the continuation probability, we obtain the path reach of a first-order node v by weighting the path reach of all corresponding higher-order nodes according to their respective relative visitation probabilities. Again, the path reach requires information on path ends. Therefore, it cannot be computed using the network model.

3   Analysis approach

So far, we have proposed eight centrality measures that allow us to quantify the influence of nodes and node sequences in path data. We established that the network model represents the least restrictive model for a set of observed paths, as transitions follow each other based on the Markov assumption and are, hence, only constrained by topology. In contrast, by computing centralities directly on a set of paths, we do not allow for any paths other than precisely those that were observed. We argued that, consequently, the network model is likely to *underfit* any restrictions present for observed paths. Similarly, we expect the centralities computed directly on the paths to *overfit* these restrictions.
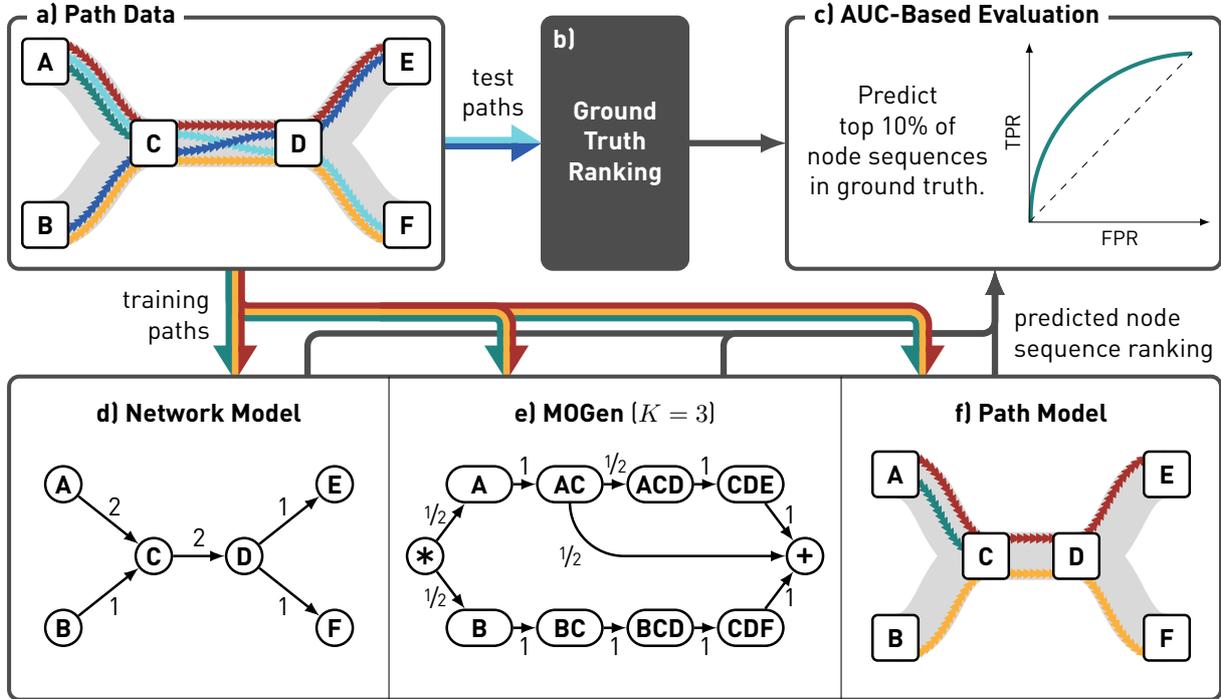
Figure 5: Overview of our approach to predict influential nodes and node sequences based on path data. We start from path data which we split into training and test sets. We learn three different models bases on the training data: (i) a network model containing all transitions from the training data, (ii) a multi-order generative model containing observed higher-order transitions up to a maximum order of K, which is determined by model selection, and (iii) a path model containing the full paths in the training set. Based on these models, we predict the influence of node or node sequences according to a broad range of centrality measures. We compare the ranking of node sequences to the ground truth rankings obtained from the test paths using AUC-based evaluation.

We hypothesise that when computing centralities based on the network or the paths directly, we misidentify the nodes that are actually influential. We further conjecture that the errors caused by underfitting and overfitting are particularly severe if the number of observed paths is low, i.e., if we have insufficient data to capture the real indirect influences present in the complex system.

We now test our hypothesis in five empirical path data sets. To this end, we compare three types of models for a set of observed paths. First, a network model containing all nodes and edges observed in the set of paths. Second, a path model which precisely captures the observed paths, i.e., the model is identical to the set of paths. Third, MOGen models with different maximum orders K that capture all higher-order patterns up to a distance of K.

Figure 5 provides an overview of our evaluation approach. We remind the reader that we aim to compare how well the different models can capture the influence of nodes in the complex system from

which we obtained the paths. As, other than the observed paths, we do not have information about the complex system, we operationalise this comparison in a prediction experiment.

3.1 Train-test split

For our prediction experiment, we first split a given set of N paths into a training and test set. Similar to balls in an urn, we treat each instance of a path as an independent observation. This means that if a path is observed i times, it is considered as i balls in the urn. To obtain our training set, we then draw n_{tr} observations. The remaining n_{te} observations comprise the test set. The normalised fractions n_{tr}/N and n_{te}/N capture the relative sizes of the training and test set.

3.2 Ground truth ranking

Next, we need to compute the real influence of nodes and node sequences in the set of test paths. We recall that the path model is the most restrictive model as it precisely and exclusively captures the set of observed paths. This means that by applying the path-based centrality measures on the set of test paths, we precisely determine the influence of nodes and node sequences. We sort the nodes and node sequences according to their influence in descending order to obtain the ground truth ranking shown in Figure 5b. This ground truth ranking serves as the prediction target for the models we train on the set of training paths in the next step.

3.3 Prediction of Influential Nodes and Node Sequences

As we argued in Section 2.2, the network and path models are the least and most restrictive models for our set of observations, respectively. The network model operates under the Markov assumption and consequently does not consider any history to compute its transition probabilities. In contrast, the path model always considers the entire history. With the MOGen model, we can adjust the amount of history considered for each transition via the model's maximum order K. With $K = 1$, a MOGen model resembles a network model with added states capturing the start- and endpoints of paths. By setting $K = l_{max}$, where l_{max} is the maximum path length in a given set of paths, we obtain a lossless representation of the path data. By varying K between 1 and l_{max}, we can adjust the model's restrictiveness between the levels of the network and the path model. We hypothesise that network and path models under- and overfit the higher-order patterns in the data, respectively, leading them to misidentify influential nodes and node sequences in out-of-sample data. Consequently, by computing node centralities based on the MOGen model, we can reduce this error.

To test this hypothesis, we train a network model, a path model, and MOGen models with $1 \leq K \leq 5$ to our set of training paths. We then apply the centrality measures introduced in Section 2.4 to compute

a ranking of nodes and node sequences according to each of the models. In a final step, we compare the computed rankings to the ground truth ranking that we computed for our test paths.

3.4 Comparison to ground truth

Before introducing our AUC-based evaluation approach, we need to spend a few more words on how we compare the predictions of the different models. While our models are all based on the same set of training paths, they make predictions for node sequences up to different lengths. For instance, in the example from Figure 1, the network model yields centralities for the first-order nodes

$$(A), \ (B), \ (C), \ (D), \ (E), \ \text{and} \ (F).$$

In contrast, a MOGen model with $K = 2$ also considers second-order nodes and thus yield centralities for

$$(A), \ (B), \ (A, C), \ (B, C), \ (C, D), \ (D, E), \ \text{and} \ (D, F).$$

Finally, the path model provides centralities for higher-order nodes with orders up to the maximum path length in the path data, i.e., up to an order of four for the example. This means that the path model yields centralities for

$$(A), \ (B), \ (A, C), \ (B, C), \ (A, C, D), \ (B, C, D), \ (A, C, D, E), \ \text{and} \ (B, C, D, F).$$

As our ground truth is based directly on the test paths, we can only compare the results of the path model directly to it.

To make the different model's predictions comparable, we can either project the predictions for node sequences back to their corresponding first-order nodes. In Section 2.4, we have provided the required projections for all centrality measures. However, the projections are lossy as they aggregate multiple higher-order nodes—i.e., node sequences—into a single first-order node. For instance, in our example from above, we would no longer be able to distinguish the influence of C as AC and BC, where in one case, a path can end and in the other, paths always continue. To obtain results that are as accurate as possible, we, therefore, opt for the alternative approach and perform our evaluation on the level of our ground truth data—i.e., the path model. In other words, instead of comparing rankings of first-order nodes, we compare rankings containing both nodes and node sequences.

We allow this comparison through an upwards projection of lower-order nodes to their matching node sequences. To this end, we match the prediction of the closest matching lower-order node $v_l \in \mathcal{L}$ as the prediction of the higher-order node $v_h \in \mathcal{H}$. Here, $\mathcal{L}$ is the set of lower-order nodes, e.g., from the

network model, whereas $\mathcal{H}$ is the set of higher-order nodes from the ground truth. We define the closest matching lower-order node v_l as the node with highest order in $\mathcal{L}$ such that v_l is a suffix of v_h. For each higher-order node, this definition allows only one lower-order node to be the closest match. However, a single lower-order node can be the closest match for more than one higher-order node. For measures that return confined quantities, such as probabilities, we follow a maximum likelihood approach and equally distribute the corresponding lower-order node's probability score across all corresponding higher-order nodes. For measures that do not return probabilities, e.g., the reach centrality, this distribution is not required. Hence, the value computed for the lower-order node can be used directly as the higher-order prediction. The upwards projection yields rankings for all models that contain precisely the set of nodes and node sequences also found in the ground truth ranking.

We evaluate how well the predictions match the ground truth using an AUC-based evaluation approach. Our approach is built on a scenario in which we aim to predict the top 10% most influential nodes and node sequences in the ground truth data. By considering this scenario, we transform the comparison of rankings into a binary classification problem, where for each node or node sequence, we predict if it belongs into the to 10% of the ground truth or not. To achieve this, we introduce a discrimination threshold $0\% \leq \alpha \leq 100\%$ that we apply to the predicted rankings. We then use all nodes and node sequences in the top $\alpha\%$ of our model's prediction to predict the top 10% ranked nodes and node sequences in the ground truth data. Trivially, for $\alpha = 0\%$, we do not predict that any node or node sequence belongs to the top 10%. Thus, we obtain a true positive rate (TPR) and a false negative rate (FPR) identical to 0. Analogously, for $\alpha = 100\%$, our predictions contain all nodes in the top 10% of the ground truth. However, we also falsely predict that all other nodes are in the top 10% resulting in TPR = FPR = 1. Ideally, if the top 10% of our predictions exactly match the ground truth we are able to achieve a true positive rate of TPR = 1 with a false positive rate of FPR = 0. As a result, the area under the corresponding ROC curve (AUC) shown in Figure 5c would be equal to 1. In contrast, deviations from a perfect ranking result in an AUC < 1. Thus, we can use the AUC of our predictions as a score of our prediction quality.

As the sampling process influences the train-test split performed in the first step of our approach our the prediction results can vary between runs. Therefore, all results reported throughout this manuscript refer to averages over at least five validation experiments.

3.5 Datasets

We test our hypothesis in five empirical path data sets containing observations from three different categories of systems: (i) user clickstreams on the Web, and (ii) travel itineraries of passengers in a

Table 1: Summary statistics for the five empirical data sets used in our evaluation.

	paths		nodes on path				network topology		
	total	unique	mean	median	min	max	nodes	links	density
BMS1	59,601	18,473	1	267	2.51	1	497	15,387	0.062
TUBE	4,295,731	32,313	2	36	7.9	7	276.0	663	0.009
SCHOOL	103,260	25,831	2	10	2.5	2	242	8,297	0.14
HOSPITAL	62,676	13,578	2	13	4.8	5	75	1,137	0.2
WORK	7,832	1,170	2	8	2.5	2	92	753	0.09

transportation network (iii) time-stamped data on social interactions. The raw data for all data sets are freely available online. We provide summary statistics for all data sets in in Table 1.

For the clickstreams, we use BMS1, which contains 59,601 clickstreams of customers of the web retailer *Gazelle.com* [6]. For the travel itineraries on a transportation network, we have TUBE, which captures 4,295,731 itineraries of London Tube passengers [34]. These data sets are directly collected in the form of paths.

In contrast, for the three data sets containing social interactions, we first need to derive paths from the recorded time-stamped data. These three data sets all originate from the *Sociopatterns* collaboration. They include (i) HOSPITAL, which captures 32,424 time-stamped proximity events between 75 patients, medical and administrative staff in a hospital recorded over a period of five days [35], (ii) WORKPLACE, which consists of 9,827 face-to-face interactions between 92 company employees recorded in an office building over a period of ten days [11] and (iii) SCHOOL which contains 77,602 proximity events between 242 individuals (232 children and 10 teachers) [30]. In Section 2.1, we showed that by setting two conditions, we can derive paths from any set of time-stamped data. The only parameter used in these conditions is the maximum time δ that cannot be exceeded between connective time-stamped events on the same path. To derive paths from our data sets, we specified δ as 800s, 1,200s, and 3,600s for SCHOOL, HOSPITAL, and WORKPLACE, respectively.

4 Results

We now present the results of our prediction experiments comparing the performance of network, path, and MOGen models to predict the influence of nodes and node sequences in out-of-sample data. For ease of discussion, we start our analysis focusing on the two data sets BMS1 and HOSPITAL. Figure 6 shows the results for the visitation probability and betweenness, closeness, and reach centrality. To compute these centralities, we do not require information on the start- and endpoint of paths. This means that equivalent measures for the network model exist. In Figure 6a, we present the ROC curves
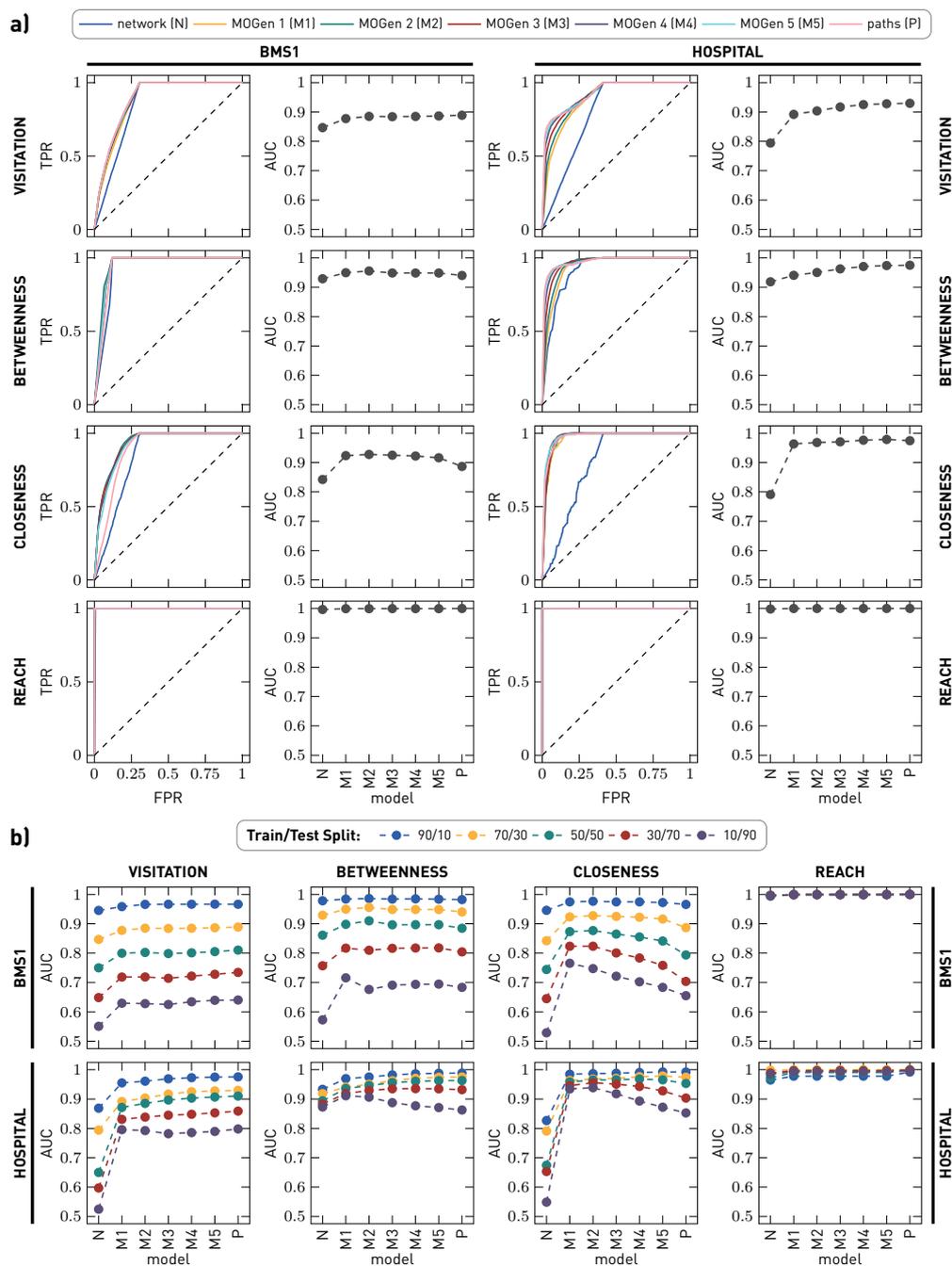
Figure 6: Prediction results for visitation probability as well as betweenness, closeness, and reach centrality for the BMS1 as well as SCHOOL data sets. **a)** shows ROC curves as well as AUC for all models for a train test-split of 70/30. **b)** shows the impact of uncertainty by shifting the train-test split from 90/10 to 10/90.

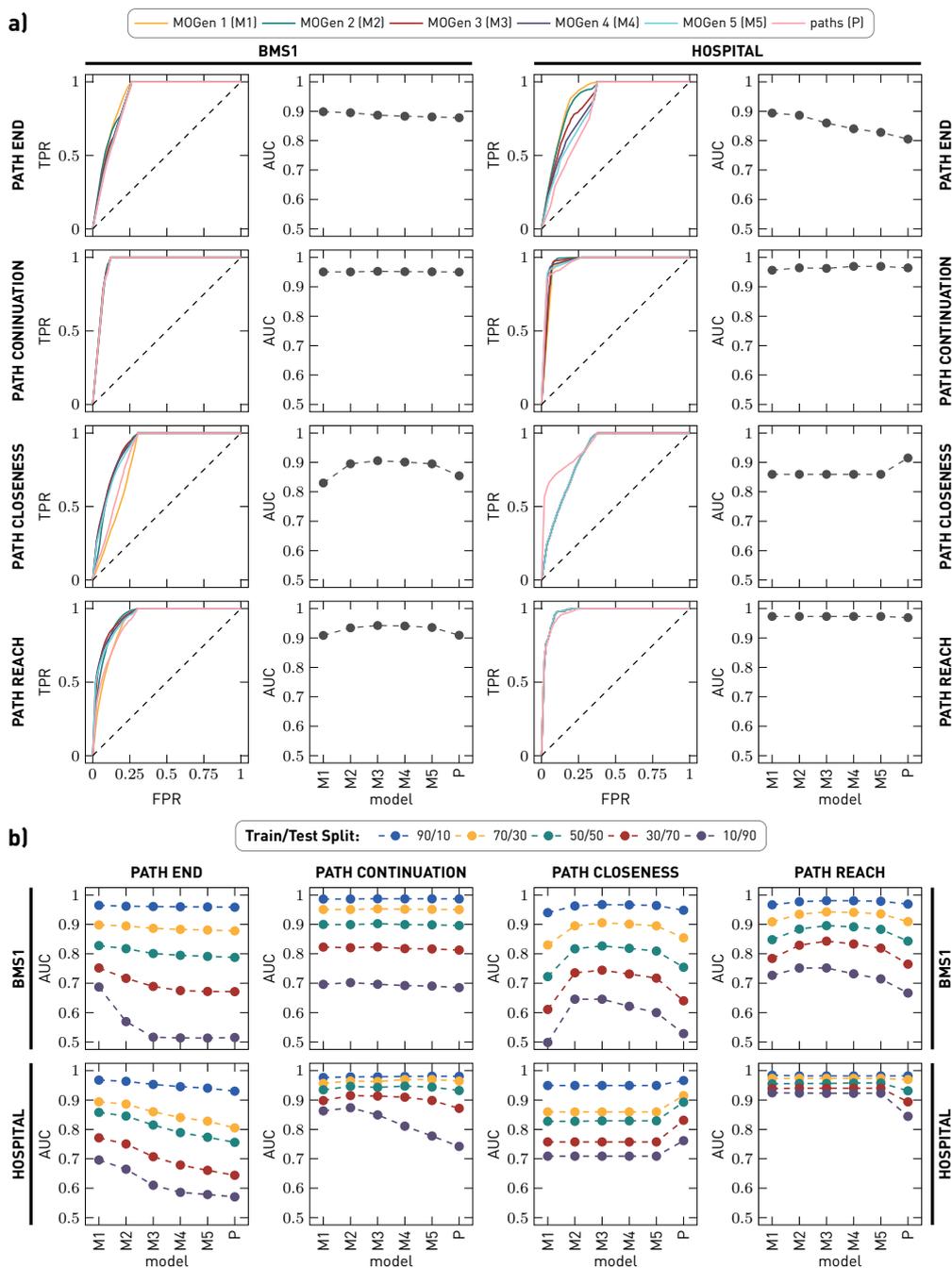**Figure 7:** Prediction results for path end, and path continuation probability as well as path closeness, and path reach centrality for the BMS1 as well as SCHOOL data sets. **a)** shows ROC curves as well as AUC for all models for a train-test split of 70/30. These measures cannot be computed for the network model. **b)** shows the impact of uncertainty by shifting the train-test split from 90/10 to 10/90.

for the BMS1 and HOSPITAL data sets using a 70/30 train-test split. In addition, we show the AUC values for the different models. The models shown on the x-axis are sorted according to the maximum distance at which they can capture indirect influences. Thus, starting from the network model (N), via the MOGen models (MK) with increasing K, the models become more restrictive until ending with the path model (P). Overall, most prediction results are excellent, showing AUC values above 0.9. For the reach centrality, we even see nearly perfect predictions for all models. That said, the network model consistently performed poorer for all other centrality measures. For the HOSPITAL data, we find that AUC generally increases for more restrictive models. For the BMS1 data, the prediction performance no longer improves for models more restrictive than M2. We find the first signs of overfitting with the closeness centrality, as the path model obtains a lower AUC score than the MOGen models.

With Figure 6b, we explore how our results change when decreasing the amount of training data provided to the model. As expected, with less training data, the AUC scores of all models decrease. However, we find that these decreases are more significant for the network and path models. As a consequence, the MOGen models outperform both the network model and the path models when only limited training data is available. This is particularly evident for the closeness centralities where we see an "inverted U-shape" in the curve displaying the AUC scores. Thus, when few data are available, our results show the potential of underfitting for network models and overfitting for path models.

In Figure 7 we show the prediction results for the path end and continuation probability, path closeness, and path reach. As these centrality measures require information on the start- and endpoints of paths, no equivalent measures for the network model exist. Therefore, we only report the performance of the MOGen models and the path model. As before, Figure 7a shows the prediction performance of the different measures with a 70/30 train-test split. Again, all models have an excellent prediction quality with average scores close to 0.9. The measures in this set incorporate more information on the indirect influence between nodes on paths. As a result, we can observe the decreased performance of the path model and MOGen models with higher K already for the 70/30 train-test split. In Figure 7b, we show that when decreasing the amount of training data, the overfitting results in a larger decrease in prediction performance.

Interestingly, comparing the predictive performance of different models for the BMS1 data, we find that a MOGen model with $K = 1$ performs best for the path end probability. However, for path closeness, the model with $K = 2$ shows substantially better performance. Simultaneously, we find that for path closeness in the HOSPITAL data, the path model consistently outperforms the MOGen models. In Table 2, we show the results for all data sets and centrality measures for a 30/70 train-test split. Here, we see that this finding is not limited to the HOSPITAL data but occurs in four out of five data sets. Finally, for the TUBE data, we find that the MOGen model with $K = 8$ and the path model yield the best performance for the first four measures. However, for the remaining measures, MOGen models

Table 2: AUC values for all models and measures on five data sets for a 30/70 train-test split. N and P indicate the network and path model, respectively. M1 through M8 are MOGen models with maximum orders between 1 and 8. Results are colour coded with the best results highlighted in green ■ and the worst results highlighted in yellow ■. The best performing model for each data set and centrality measure is framed in grey ■.

		N	M1	M2	M3	M4	M5	M6	M7	M8	P
BMS1	visitation	0.6486	0.7185	0.7188	0.7143	0.7217	0.7280	—	—	—	0.7343
	betweenness	0.7569	0.8169	0.8096	0.8163	0.8173	0.8177	—	—	—	0.8042
	closeness	0.6449	0.8234	0.8235	0.8006	0.7834	0.7582	—	—	—	0.7035
	reach	0.9963	0.9993	0.9994	0.9995	0.9994	0.9995	—	—	—	0.9999
	path end	—	0.7517	0.7166	0.6891	0.6749	0.6720	—	—	—	0.6714
	path continuation	—	0.8228	0.8206	0.8234	0.8176	0.8165	—	—	—	0.8126
	path closeness	—	0.6109	0.7354	0.7442	0.7313	0.7173	—	—	—	0.6402
	path reach	—	0.7841	0.8291	0.8429	0.8332	0.8191	—	—	—	0.7648
SCHOOL	visitation	0.6191	0.7031	0.7568	0.7541	0.7519	0.7526	—	—	—	0.7530
	betweenness	0.7963	0.8331	0.8407	0.8357	0.8335	0.8326	—	—	—	0.8270
	closeness	0.6198	0.8069	0.8221	0.7806	0.7628	0.7584	—	—	—	0.7521
	reach	0.9968	0.9993	0.9997	0.9996	0.9997	0.9996	—	—	—	0.9999
	path end	—	0.6521	0.6270	0.5641	0.5677	0.5703	—	—	—	0.5719
	path continuation	—	0.8100	0.7968	0.7767	0.7619	0.7573	—	—	—	0.7552
	path closeness	—	0.5997	0.5997	0.5997	0.5997	0.5997	—	—	—	0.6585
	path reach	—	0.8547	0.8547	0.8547	0.8547	0.8547	—	—	—	0.7462
HOSPITAL	visitation	0.5971	0.8309	0.8385	0.8451	0.8482	0.8530	—	—	—	0.8590
	betweenness	0.8828	0.9191	0.9291	0.9351	0.9355	0.9347	—	—	—	0.9320
	closeness	0.6533	0.9459	0.9556	0.9509	0.9429	0.9279	—	—	—	0.9034
	reach	0.9887	0.9966	0.9967	0.9967	0.9967	0.9967	—	—	—	0.9989
	path end	—	0.7713	0.7505	0.7071	0.6788	0.6608	—	—	—	0.6440
	path continuation	—	0.8979	0.9151	0.9134	0.9096	0.8983	—	—	—	0.8716
	path closeness	—	0.7575	0.7575	0.7575	0.7575	0.7575	—	—	—	0.8311
	path reach	—	0.9390	0.9401	0.9401	0.9401	0.9401	—	—	—	0.8936
WORK	visitation	0.5613	0.8000	0.8368	0.8499	0.8509	0.8523	—	—	—	0.8530
	betweenness	0.7973	0.8542	0.8290	0.8406	0.8416	0.8418	—	—	—	0.8829
	closeness	0.5886	0.8495	0.8445	0.8349	0.8342	0.8345	—	—	—	0.8819
	reach	0.9635	0.9136	0.9046	0.9110	0.9130	0.9137	—	—	—	0.9882
	path end	—	0.6955	0.6844	0.6842	0.6863	0.6877	—	—	—	0.6438
	path continuation	—	0.7431	0.7751	0.7651	0.7648	0.7633	—	—	—	0.7894
	path closeness	—	0.6785	0.6809	0.6812	0.6812	0.6812	—	—	—	0.7685
	path reach	—	0.8862	0.8847	0.8828	0.8831	0.8831	—	—	—	0.8419
TUBE	visitation	0.6070	0.8042	0.8978	0.9178	0.9313	0.9395	0.9368	0.9421	0.9465	0.9650
	betweenness	0.7634	0.8223	0.9008	0.9241	0.9393	0.9474	0.9453	0.9500	0.9542	0.9700
	closeness	0.5497	0.7415	0.8679	0.9046	0.9329	0.9598	0.9707	0.9742	0.9749	0.9786
	reach	0.9239	0.9254	0.9228	0.9241	0.9243	0.9238	0.9920	0.9928	0.9932	0.9903
	path end	—	0.7995	0.7974	0.7721	0.7378	0.6965	0.6023	0.5614	0.5277	0.5719
	path continuation	—	0.6920	0.7179	0.7269	0.7196	0.7196	0.6809	0.6757	0.6683	0.6704
	path closeness	—	0.8456	0.7914	0.7581	0.7302	0.7114	0.6530	0.6537	0.6684	0.9106
	path reach	—	0.7093	0.8787	0.8996	0.9131	0.9101	0.9005	0.8933	0.8845	0.8430

with lower K perform better. Thus, we conclude that the selection of the most suitable model depends not only on the data but also on the centrality measure that we are trying to capture. We will further explore this finding in future research.

The data sets in Table 2 are sorted according to the fraction of total paths over the unique paths in the data set. As shown in Table 1 the BMS1 data contain 59,601 total paths of which 18,473 are unique. This means that, on average, each unique path is observed 3.2 times. These counts increase to 4 for SCHOOL, 4.6 for HOSPITAL, 6.7 for WORK and 132.9 for TUBE. As we can see in Table 2 the performance of the path model improves and even exceeds the MOGen model when an increasing amount of observations per unique path. This shows that the error we found with fewer observations is indeed due to overfitting. In turn, if we have a sufficient number of observations, we can compute the centralities on the path data directly. However, we confirm that if the number of observations is insufficient, the path model overfits the patterns in the training data and consequently performs worse on out-of-sample data. How many observations are required to justify using the path model depends on the number of unique paths contained in the data set.

In conclusion, our results support our hypothesis. By not capturing the higher-order patterns present in path data and not considering the start- and endpoints of paths, the network model underfits the patterns present in path data. Similarly, if we have insufficient observations, the path model overfits these patterns. Consequently, when using either model to rank the influence of nodes and node sequences in path data, we obtain rankings that are not consistent with future out-of-sample observations. Prediction performance can be significantly improved by using MOGen models that prevent underfitting by capturing higher-order patterns up to a distance of K while simultaneously preventing overfitting by ignoring patterns at larger distances.

5 Conclusion

Paths capture higher-order patterns, i.e., indirect influences, between elements of complex systems not captured by network topology. To accurately capture the influence of nodes and node sequences, we must accurately account for these higher-order patterns present in our data. However, not all higher-order patterns observed in a set of paths are representative of the actual dynamics of the underlying system. In other words, by computing centralities on the full paths, we are likely to overfit higher-order patterns and attribute centrality scores to nodes and node sequences different to the ones we obtain when further observing the system and collecting additional paths. Therefore, we require a model that captures only those higher-order patterns for which there is sufficient statistical evidence in the data. We argued that the multi-order generative model MOGen is an ideal model for this pur-

pose as it captures higher-order patterns in paths up to a given length while simultaneously including representations for the start and end of paths.

Based on the MOGen representation, we proposed measures to quantify the influence of both nodes and node sequences in path data according to eight different notions of centrality. Our centrality measures range from simple concepts like the visitation probability to complex measures such as path reach. For all centrality measures, we also proposed equivalent measures computed directly on path data. While equivalent measures exist for the simple notions of centrality, networks cannot represent the start and end of paths and, hence, cannot represent the full information contained in a path. Consequently, for the more complex measures, no network equivalents exist.

We hypothesised that networks models underfit and path models overfit higher-order patterns in path data. Therefore, by computing the centralities of nodes or node sequences according to these models, we misidentify influential nodes. By using MOGen, we can avoid both under- and overfitting. Thus, when computing centralities for MOGen models, we obtain rankings that better represent influential nodes in out-of-sample data.

Using a prediction experiment with five empirical data sets, we found evidence that supports our hypothesis. Centralities computed on the MOGen and the path models consistently outperform those based on the network model. This result highlights the potential consequences of applying networks—the most popular model for relational data—to sequential data. Similarly, MOGen-based centralities generally outperform or match those computed using the path model. The performance difference is greater if the ratio between the number of observed paths and the number of unique paths in a data set decreases. Thus, the larger the variance in the set of observed paths, the larger the potential for overfitting when using a path model to identify central nodes and node sequences in the data. This effect decreases when increasing the amount of training data and consequently decreasing the generalisation error. However, for many real-world systems such as human interactions, the range of possible interactions and thus the number of possible paths is extensive, and interaction data is either costly to obtain or limited in availability. In these cases, our MOGen-based centrality measures provide significantly more accurate predictions on the true influential nodes and node sequences compared to both the network- and path-based measures.

In future work, we will further explore the mechanisms that cause the performance of our models to depend not only on the data set but also on the type of centrality they are aiming to capture.

Archival and Reproducibility

Sources for all data used in this paper are provided. All other data supporting the plots within this paper are available upon reasonable request. A parallel implementation of the MOGen model is available at `https://github.com/pathpy/pathpy3`.

Acknowledgements

References

[1] Arasu, A.; Novak, J.; Tomkins, A.; Tomlin, J. (2002). PageRank computation and the structure of the web: Experiments and algorithms. In: *Proceedings of the Eleventh International World Wide Web Conference, Poster Track.* pp. 107–117.

[2] Battiston, F.; Cencetti, G.; Iacopini, I.; Latora, V.; Lucas, M.; Patania, A.; Young, J.-G.; Petri, G. (2020). Networks beyond pairwise interactions: structure and dynamics. *Physics Reports* .

[3] Bavelas, A. (1950). Communication patterns in task-oriented groups. *The journal of the acoustical society of America* **22(6)**, 725–730.

[4] Boccaletti, S.; Latora, V.; Moreno, Y.; Chavez, M.; Hwang, D.-U. (2006). Complex networks: Structure and dynamics. *Physics reports* **424(4-5)**, 175–308.

[5] Borgatti, S. P. (2005). Centrality and network flow. *Social networks* **27(1)**, 55–71.

[6] Brodley, C.; Kohavi, R. (2000). KDD-Cup 2000 homepage.

[7] Chung, F. R.; Graham, F. C. (1997). *Spectral graph theory.* No. 92, American Mathematical Soc.

[8] Edler, D.; Bohlin, L.; Rosvall, M. (2017). Mapping higher-order network flows in memory and multilayer networks with infomap. *Algorithms* **10(4)**, 112.

[9] Floyd, R. W. (1962). Algorithm 97: shortest path. *Communications of the ACM* **5(6)**, 345.

[10] Freeman, L. C. (1977). A set of measures of centrality based on betweenness. *Sociometry* , 35–41.

[11] Génois, M.; *et al.* (2015). Data on face-to-face contacts in an office building suggest a low-cost vaccination strategy based on community linkers. *Network Science* **3(3)**, 326–347.

[12] Gote, C.; Casiraghi, G.; Schweitzer, F.; Scholtes, I. (2020). Predicting Sequences of Traversed Nodes in Graphs using Network Models with Multiple Higher Orders.

[13] Krieg, S. J.; Robertson, D. H.; Pradhan, M. P.; Chawla, N. V. (2020). Higher-order Networks of Diabetes Comorbidities: Disease Trajectories that Matter. In: *2020 IEEE International Conference on Healthcare Informatics (ICHI)*. IEEE, pp. 1–11.

[14] Lambiotte, R.; Rosvall, M.; Scholtes, I. (2019). From networks to optimal higher-order models of complex systems. *Nature physics* **15(4)**, 313–320.

[15] Lambiotte, R.; Salnikov, V.; Rosvall, M. (2015). Effect of memory on the dynamics of random walks on networks. *Journal of Complex Networks* **3(2)**, 177–188.

[16] LaRock, T.; Nanumyan, V.; Scholtes, I.; Casiraghi, G.; Eliassi-Rad, T.; Schweitzer, F. (2020). Hypa: Efficient detection of path anomalies in time series data on networks. In: *Proceedings of the 2020 SIAM International Conference on Data Mining*. SIAM, pp. 460–468.

[17] Marchiori, M.; Latora, V. (2000). Harmony in the small-world. *Physica A: Statistical Mechanics and its Applications* **285(3-4)**, 539–546.

[18] Myall, A. C.; Peach, R. L.; Weiße, A. Y.; Mookerjee, S.; Davies, F.; Holmes, A.; Barahona, M. (2021). Network memory in the movement of hospital patients carrying antimicrobial-resistant bacteria. *Applied Network Science* **6(1)**, 1–23.

[19] Page, L.; Brin, S.; Motwani, R.; Winograd, T. (1999). *The PageRank citation ranking: Bringing order to the web.* Tech. rep., Stanford InfoLab.

[20] Palla, G.; Páll, N.; Horváth, A.; Molnár, K.; Tóth, B.; Kováts, T.; Surján, G.; Vicsek, T.; Pollner, P. (2018). Complex clinical pathways of an autoimmune disease. *Journal of Complex Networks* **6(2)**, 206–214.

[21] Peixoto, T. P.; Rosvall, M. (2017). Modelling sequences and temporal networks with dynamic community structures. *Nature communications* **8(1)**, 1–12.

[22] Perri, V.; Scholtes, I. (2020). HOTVis: Higher-Order Time-Aware Visualisation of Dynamic Graphs. In: D. Auber; P. Valtr (eds.), *Graph Drawing and Network Visualization - 28th International Symposium, GD 2020, Vancouver, BC, Canada, September 16-18, 2020, Revised Selected Papers*. Springer, vol. 12590 of *Lecture Notes in Computer Science*, pp. 99–114.

[23] Rosvall, M.; Bergstrom, C. T. (2008). Maps of random walks on complex networks reveal community structure. *Proceedings of the National Academy of Sciences* **105(4)**, 1118–1123.

[24] Rosvall, M.; Esquivel, A. V.; Lancichinetti, A.; West, J. D.; Lambiotte, R. (2014). Memory in network flows and its effects on spreading dynamics and community detection. *Nature communications* **5(1)**, 1–13.

[25] Saebi, M.; Ciampaglia, G. L.; Kaplan, L. M.; Chawla, N. V. (2020). HONEM: learning embedding for higher order networks. *Big Data* **8(4)**, 255–269.

[26] Saebi, M.; Xu, J.; Kaplan, L. M.; Ribeiro, B.; Chawla, N. V. (2020). Efficient modeling of higher-order dependencies in networks: from algorithm to application for anomaly detection. *EPJ Data Science* **9(1)**, 15.

[27] Scholtes, I. (2017). When is a network a network? Multi-order graphical model selection in pathways and temporal networks. In: *Proceedings of the 23rd ACM SIGKDD international conference on knowledge discovery and data mining.* pp. 1037–1046.

[28] Scholtes, I.; Wider, N.; Garas, A. (2016). Higher-order aggregate networks in the analysis of temporal networks: path structures and centralities. *The European Physical Journal B* **89(3)**, 1–15.

[29] Scholtes, I.; Wider, N.; Pfitzner, R.; Garas, A.; Tessone, C. J.; Schweitzer, F. (2014). Causality-driven slowdown and speed-up of diffusion in non-Markovian temporal networks. *Nature communications* **5(1)**, 1–9.

[30] Stehlé, J.; Voirin, N.; Barrat, A.; Cattuto, C.; Isella, L.; Pinton, J.-F.; Quaggiotto, M.; Van den Broeck, W.; Régis, C.; Lina, B.; *et al.* (2011). High-resolution measurements of face-to-face contact patterns in a primary school. *PloS one* **6(8)**, e23176.

[31] Strogatz, S. H. (2001). Exploring complex networks. *nature* **410(6825)**, 268–276.

[32] Tao, J.; Xu, J.; Wang, C.; Chawla, N. V. (2017). HoNVis: Visualizing and exploring higher-order networks. In: *2017 IEEE Pacific Visualization Symposium (PacificVis).* IEEE, pp. 1–10.

[33] Torres, L.; Blevins, A. S.; Bassett, D. S.; Eliassi-Rad, T. (2020). The why, how, and when of representations for complex systems. *arXiv preprint arXiv:2006.02870* .

[34] Transport for London (2014). Rolling Origin and Destination Survey (RODS) database.

[35] Vanhems, P.; Barrat, A.; Cattuto, C.; Pinton, J.-F.; Khanafer, N.; Regis, C.; Kim, B.-A.; Comte, B.; Voirin, N. (2013). Estimating Potential Infection Transmission Routes in Hospital Wards Using Wearable Proximity Sensors. *PLoS ONE* **8**.

[36] Xu, J.; Wickramarathne, T. L.; Chawla, N. V. (2016). Representing higher-order dependencies in networks. *Science advances* **2(5)**, e1600028.

[37] Zhang, Y.; Garas, A.; Scholtes, I. (2020). Higher-order models capture changes in controllability of temporal networks. *Journal of Physics: Complexity* .